Applied Surface Science 579 (2022) 152121

Contents lists available at ScienceDirect

Applied Surface Science

journal homepage: www.elsevier.com/locate/apsusc

Full Length Article

Cobalt oxide decorated porous silica particles: Structure and activity relationship in the catalytic oxidation of carbon monoxide

Daniil A. Eurov [a,*], Tatiana N. Rostovshchikova [b], Marina I. Shilina [b], Demid A. Kirilenko [a], Maria V. Tomkovich [a], Maria A. Yagovkina [a], Olga V. Udalova [c], Igor Yu. Kaplin [b], Igor A. Ivanin [b], Dmitry A. Kurdyukov [a]

[a] Ioffe Institute, 194021 St. Petersburg, Russia
[b] Lomonosov Moscow State University, Department of Chemistry, 119991 Moscow, Russia
[c] Semenov Federal Research Center for Chemical Physics, 119991 Moscow, Russia

ARTICLE INFO

Keywords:
Silica particles
Co-SiO_2 composites
Porosity
Catalytic activity
CO oxidation
CO–PROX

ABSTRACT

Porous (0.6–30 nm) and non-porous spherical silica nanoparticles are synthesized. These silicas with different morphologies are decorated with cobalt (2.9 wt%) using $Co(NO_3)_2{\cdot}6H_2O$ as precursor. Co-SiO_2 particles are studied by N_2 sorption, TEM, XRD, XPS, FTIR and TPR-H_2 methods. Specific surface area (SSA) of the prepared materials is 10–1200 m^2/g. The main crystalline phase is identified as Co_3O_4. The activity of Co-SiO_2 composites in the CO oxidation and preferential oxidation of CO (PROX) in a H_2-rich gas mixture improves with increasing atomic ratios of Co/Si and Co^{3+}/Co^{2+} on the silica surface. Catalysts with the large mesopores containing mainly Co^{2+} are the least active. Co-SiO_2 composites based on synthetic opal grown by sedimentation of non-porous silica particles with the lowest SSA demonstrate the highest catalytic activity. The CO conversion reaches 100% at 150 °C in the absence of hydrogen, while in PROX the 90% conversion of CO is achieved at 170 °C. The large Co_3O_4 aggregates between non-porous spherical silica particles of opal are the most active and stable during CO-PROX reaction. The lower interaction of Co_3O_4 nanoparticles with this support promotes the stabilization of the oxidized state Co^{3+} and provides a higher yield of CO_2 in CO-PROX reaction.

1. Introduction

Oxidation of carbon monoxide with oxygen is of interest in terms of the development of fundamental concepts of heterogeneous catalysis [1,2]. At the same time, the search for inexpensive and effective catalysts for the process, especially for CO-PROX in a H_2-rich gas mixture, is a significant practical problem [3,4]. Cobalt oxides attract the attention due to the high activity in CO oxidation, which is only slightly inferior compared to catalysts based on noble metals [2,5–7]. Researchers are looking for the most effective structures of nanosized cobalt oxides [8] and promoters enhancing their catalytic ability and stability [9,10]. The best results are achieved with the combined use of cobalt and copper/cerium oxides [11,12]. Cerium oxides, along with less active ZrO_2, Al_2O_3, SiO_2 and zeolites, are used as supports for the stabilization of cobalt oxides [13–16]. In all cases, the characteristics of the catalysts are extremely dependent on the method of synthesis, its conditions, the nature and concentration of the precursor, the carrier used, etc. [16–19]. The literature discusses the participation of Co_3O_4 and CoO oxides, as well as mixed-valence cobalt-oxo complexes (Co^{3+}–O–Co^{2+}) in the activation of oxygen and the oxidation of carbon monoxide [9,10,19–21]. In most cases, the catalytic activity correlates with the Co^{3+}/Co^{2+} ratio. The high activity and stability of Co-modified zeolites of the ZSM-5 type are associated with the formation in the zeolite channels of cobalt-oxo cations active in catalysis [16].

Silicas due to their unique characteristics, such as high specific surface area (>1000 m^2/g), large pore volume (up to 1 cm^3/g), variable morphology and pore size, ease of surface modification, both external and internal, chemical inertness and temperature stability, are widely used as adsorbents, catalyst supports, molecular sieves, chemical sensors, nanoreactors [22,23]. The use of silica to stabilize cobalt oxides remains a challenge due to some advantages and disadvantages of this support. Silica allows avoiding undesirable interactions of cobalt oxide with support [2]. The strong oxide-oxide interaction with, e.g. Al_2O_3 or TiO_2 leads to the formation of non-active phases and reduces the activity

* Corresponding author.
E-mail address: edan@mail.ru (D.A. Eurov).

https://doi.org/10.1016/j.apsusc.2021.152121
Received 22 September 2021; Received in revised form 25 November 2021; Accepted 1 December 2021
Available online 5 December 2021

of Co_3O_4 in CO oxidation [24,25]. But the weak cobalt oxide - silica interaction reduces the thermal stability of cobalt supported catalysts. To overcome this problem novel forms of silica are used. Mesoporous silicas are highly suitable and efficient to attain a good dispersion of active phases and promoters, owing to their high specific surface area and mesoporous structure, particularly, SBA-15 [11] and MCM-41 [15]. Promising activity was found for nanoclusters of Co_3O_4 inserted in the mesoporous SBA-15 [26,27]. No deactivation after calcination at 400 °C was observed for this catalyst, whereas CoO_x impregnated in silica lost half of the activity. Other aspects that should be taken into account are an accessibility of active phase for reactants in the pore structure of silica and the cobalt oxide reducibility. Co-MCM-41, which contains mainly cobalt incorporated into the framework, has been used as a heterogeneous, low cost, and easily recyclable catalyst for the oxidation of renewable substrates [28]. This material has shown better performance in the terpene oxidation that SiO_2 prepared by the conventional sol–gel method. For the further application of Co/SiO_2 in catalysis, a detailed study of the effect of silica morphology on their catalytic behavior is required. Silica porous structure becomes one of the key factors determining the cobalt oxide particles' size, their distribution in silica structure and the cobalt electronic state.

In this work, nanosized silica particles of various morphologies were used as supports for the synthesis of Co-containing catalysts. The methods developed by the authors of this work for the synthesis of spherical silica particles with a size of 400–800 nm made it possible to vary their specific surface area within a wide range from 11 to 1620 m^2/g [29–32]. The catalytic properties of cobalt oxides introduced into the amorphous silica particles are compared in the CO oxidation with oxygen both in an inert atmosphere and in the presence of hydrogen. The aim of the work was to establish the effect of silica morphology on the structure and properties of the obtained Co-SiO_2 composites.

2. Experimental

2.1. Synthesis of samples

Porous amorphous silicas of 4 types consisting of spherical particles were used as supports: synthetic opal formed from close-packed non-porous particles (*SiO_2-n*), mesoporous particles (*SiO_2-m*), micro-mesoporous particles (*SiO_2-mm*) and particles with large mesopores (*SiO_2-lm*). The procedure for the samples' preparation is schematically depicted in Scheme 1.

The synthesis of *SiO_2-n* particles with a diameter of 760 ± 20 nm was carried out via hydrolysis of tetraethoxysilane (TEOS) in a mixture NH_3–H_2O–C_2H_5OH [29]. The synthesized particles were annealed in air at 900 °C and then redispersed in deionized water. Opals were grown from an aqueous suspension of *SiO_2-n* particles by sedimentation. The resulting sediment was dried at a temperature of 100 °C and annealed at 800 °C. The volume available for filling was up to 26% of the total opal volume, and the specific surface area (according to the Brunauer-Emmett-Teller (BET) method) was 11 m^2/g.

Particles of *SiO_2-m* were synthesized via basic hydrolysis of TEOS in a mixture NH_3–H_2O–C_2H_5OH in the presence of cetyltrimethylammonium bromide (CTAB). The molar ratio of the reagents TEOS:C_2H_5OH:H_2O:NH_3:CTAB was 1:250:45:400:0.25, respectively. To remove organic compounds the synthesized particles were annealed in air at 550 °C. The diameter of the particles was 390 ± 35 nm, pore size – 2.5–3.7 nm, pore volume – 0.48 cm^3/g, specific surface area (BET) – 735 m^2/g. The procedure for the synthesis of *SiO_2-m* is described in [30].

Particles of *SiO_2-mm* possessing pores of 0.9–3.5 nm in size were synthesized via basic hydrolysis of silicon-containing precursors (TEOS and [3-(methacryloyloxy)propyl]trimethoxysilane (MPTMOS)) in a mixture NH_3–H_2O–C_2H_5OH–CTAB [31]. The molar ratio of the reagents (TEOS + 20 mol.% MPTMOS):NH_3:H_2O:C_2H_5OH:CTAB was 1:60:370:230:0.2, respectively. To remove organics the synthesized particles were washed with an alcoholic solution of HCl (0.01 M) and then were annealed in a flow of O_2 at 400 °C for 5 h. The outer diameter, specific surface area and pore volume of *SiO_2-mm* were 510 ± 50 nm,

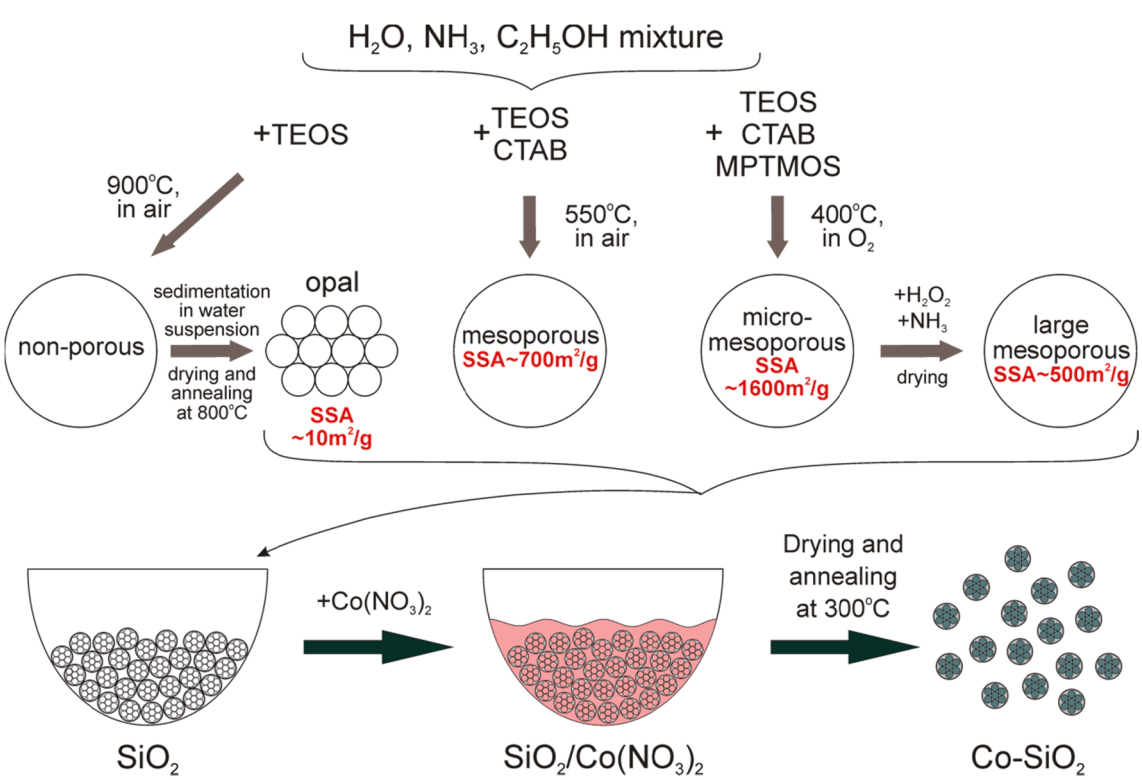

Scheme 1. Schematic illustration of the Co-SiO_2 composites preparation.

1620 m^2/g (BET) и 0.69 cm^3/g, respectively.

To increase the size of mesopores to 5–25 nm, a freshly prepared aqueous solution (50 mL) of H_2O_2 and NH_3 with concentrations of 3 M and 10 M, respectively, were added to a glass beaker containing a weighed portion of *SiO2-mm* (0.5 g) [32]. The resulting suspension was heated with stirring to a temperature of 65 °C and kept for 1 h, and then it was cooled in air to room temperature. The particles thus treated were washed three times in deionized water and dried at 100 °C. The outer diameter of the particles did not change. The specific surface area (BET) and pore volume of the obtained *SiO2-lm* particles were 515 m^2/g and 0.79 cm^3/g, respectively.

The introduction of cobalt oxide into the pores of the opal and SiO_2 particles included several steps. First, a weighed portion of silica was impregnated with a 2 M aqueous solution of $Co(NO_3)_2{\cdot}6H_2O$ under ambient conditions, then dried at 70 °C. Thereafter, the temperature was increased to 350 °C (with a 10 °C/min step). Then, heat treatment was carried out at 350 °C under normal conditions for 3 h. The Co content in all Co-SiO_2 composites was 2.9 wt% (based on the mass ratio of silica and cobalt nitrate).

2.2. Characterization

The Co content was analyzed by total reflection X-ray fluorescence (TXRF) on S2 PICOFOX energy-dispersive spectrometer (Bruker Nano, Germany). Mo Kα radiation was used for sample excitation. Co Kα (6.9 keV) was used for measurements. A mixture of concentrated HCl and HF was used to dissolve *Co-SiO2*. The experimental values of Co-content in all *Co-SiO2* composites are listed in Table 1.

The porous structure of samples was studied with a Micromeritics ASAP 2020 analyzer at a temperature of 77 K, with nitrogen as the adsorbate. The specific surface area was calculated by the BET method, the pore volume was measured at relative pressure $P/P_0 = 0.995$. The pore size distribution was found using the nonlocal density functional theory (NLDFT).

The phase composition of Co-SiO_2 was analyzed by powder X-ray diffraction (XRD) analysis using a D2 Phaser, Bruker (CuKα radiation). Transmission electron microscopy (TEM) studies were performed using a Jeol JEM-2100F microscope (accelerating voltage 200 kV, point-to-point resolution 0.19 nm) equipped with Bruker XFlash 6 T-30 energy dispersive X-ray (EDX) spectrometer.

X-ray photoelectron spectroscopy (XPS) analysis of the samples before and after catalysis was performed with an Axis Ultra DLD spectrometer (Kratos Analytical Limited, UK) with a monochromatic Al Kα source ($h\nu = 1486.7$ eV, 150 W). All data were acquired at a pass energy of 40 and 160 eV for high-resolution and survey spectra, respectively. Kratos charge neutralizer system was used, Si2p spectra with a binding energy of 103.6 eV characteristic for silica were used for calibration.

The infrared spectra (FTIR) of the samples were obtained on an Infralum FT-801 (Lyumeks–Sibir, Russia) Fourier spectrometer with a resolution of 2 cm^{-1}. One milligram of each powder sample was diluted with 75 mg of potassium bromide (KBr) powder.

Temperature-programmed reduction (TPR-H_2) of *Co-SiO2* catalysts was performed using a USGA-101 (UNISIT, Russia) chemisorption analyzer. The samples (0.06 g) were preliminary heated at 300 °C in Ar flow for 0.5 h, than cooled down to 30 °C. The reduction was performed in a diluted hydrogen flow (30 mL/min, 5 % H_2, 95 %n Ar) at a heating rate of 10 °C/min from 30 to 850 °C.

Table 1
Structural parameters of Co-SiO_2 composites.

Support	SiO_2-*n*	SiO_2-*mm*	SiO_2-*m*	SiO_2-*lm*
Co, wt. %	2.9	3.2	2.9	3.1
S (BET-equivalent), m^2/g Co-SiO_2/SiO_2	10/11	1205/1620	695/735	410/515
Total volume of pores (inside the silica particles), cm^3/g Co-SiO_2/SiO_2	0.025/0.03	0.54/0.69	0.47/0.48	0.60/0.79
Pore width (NLDFT), nm Co-SiO_2/SiO_2	n/a	0.8–3.0/0.9–3.5	2.2–6.0/2.5–3.7	0.8–2 ; 5–30/0.8–5 ; 7–30
Silica particle diameter, nm	760 ± 20	510 ± 50	390 ± 35	500 ± 40
CSA of Co_3O_4, nm	25.1 ± 0.3	4.7 ± 0.1	5.1 ± 0.1	7.8 ± 0.1

2.3. Catalytic tests

Co-SiO2 catalysts were tested in a quartz fixed-bed flow reactor (i.d. = 6 mm) operated at atmospheric pressure at temperatures of 50–250 °C in heating–cooling modes (2–4 cycles). Temperature control was carried out using a Ursamar-RK42 programmer (Germany). The samples were preliminarily heated in a flow of helium at 370 °C for 30 min. The reagent gas consisted of CO: O_2: He = 1: 1: 98 vol% or CO:O_2:H_2:He = 1:1:49:49 vol% for CO oxidation and PROX, respectively; 250 mg of catalyst (40–60 mesh) mixed with 250 mg of quartz sand were used. The reactants and products were analyzed on line by GC (thermal conductivity detector; packed column Porapak Q 1 m long, a column temperature of 30 °C, a flow rate of 10 cm^3/min) using a Crystal 2000 chromatograph. A software package Ecochrome was used for data processing. Absolute sensitivity for all analyzed substances did not exceed 10^{-3} vol%. For the comparison of catalytic activity of different samples the temperature dependencies of the steady-state CO conversion as well as temperatures of the 10% and 50% conversion of CO (T_{10} and T_{50}) were used.

3. Results and discussion

3.1. Structural characteristics of Co-SiO2 composites

Fig. 1a shows nitrogen adsorption isotherms at 77 K of *Co-SiO2* composites. The isotherms of *Co-SiO2-m*, *Co-SiO2-mm* and *Co-SiO2-lm* composites have a step-like form characteristic of M41S materials [23] and belong to type IV [33]. The isotherms of the *Co-SiO2-m* and *Co-SiO2-lm* composites exhibit a hysteresis at $P/P_0 > 0.4$, which is due to capillary condensation in mesopores>5 nm. The isotherm of the *Co-SiO2-n* composite is characteristic of non-porous materials and belongs to type III [33]. Nevertheless, there are two types of interparticle pores between close-packed spherical *SiO2-n* particles in opal: octahedral (O) and tetrahedral (T). At point contacts between *SiO2-n* particles, the diameter of hypothetical spheres inscribed in the pores is: ~ 0.41 D (for O-pores) and ~ 0.23 D (for T-pores), where D – diameter of *SiO2-n* particles. The diameter of the bottlenecks of the horn-shaped channels connecting the O- and T-pores is ~ 0.15 D [34]. At D = 760 nm, the interparticle pore size in the opal is 100–300 nm. These pores are not detectable by the method of low-temperature nitrogen adsorption since capillary condensation occurs in them at $P/P_0 \sim 0.99$.

The results of calculating the pore size distribution performed by the NLDFT method are shown in Fig. 1b. They are also listed in Table 1 together with the values of specific surface area (calculated by BET in the range $0.05 \le P/P_0 \le 0.20$) and pore volume (at $P/P_0 \sim 0.995$) in comparison with the characteristics of initial silicas. Reference characteristics for initial silicas were calculated from the data shown in Fig. S1. Based on the comparison of these data (Figs.1, S1, Table 1) it can be concluded that the porous structure of the composites after the introduction of cobalt oxide is preserved, but a redistribution of cobalt oxide between outer and inner silica surface leads to a decrease in the specific surface area and some changes in pore volume of SiO_2. The pore volume could change due to two factors: the inclusion of cobalt species inside the pores and the deposition of cobalt oxide particles on the outer surface closing some pores. The most noticeable changes are seen for *SiO2-lm* and *SiO2-mm* materials. The introduction of cobalt into *SiO2-lm* leads

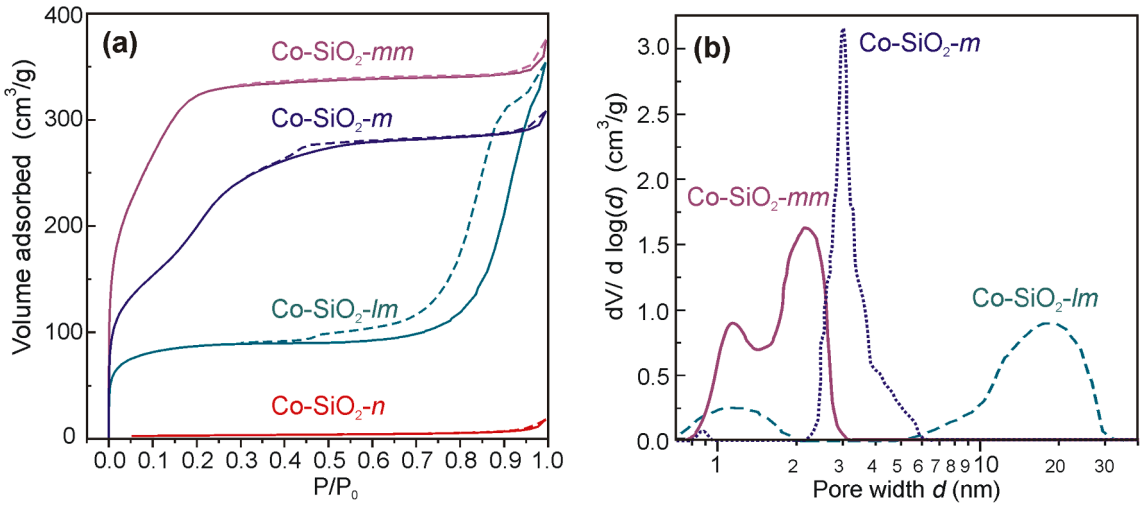

Fig. 1. Nitrogen adsorption–desorption isotherms at 77 K (a) and pore size distribution calculated by NLDFT (b) of Co-SiO_2 composites.

to a decrease in the total surface area, pore volume and in the size both of small pores (from 0.8–5 nm to 0.8–2 nm) and large pores (from 7–30 to 5–30 nm). In contrast to this, the pore sizes of *Co-SiO₂-mm* practically did not change upon the introduction of cobalt, but the surface and pore volume also decreased significantly, which indicates that a significant part of the oxide particles are located on the outer silica surface. Some enlargement in the pore size for the *Co-SiO₂-m* sample (from 2.5–3.7 nm to 2.2–6.0 nm) indicates that cobalt oxide probably penetrates into the pores. At the same time, the total pore volume and surface have changed insignificantly. As can be seen from the TEM below, the content of cobalt oxide particles on the silica surface is different.

The presence of crystalline Co_3O_4 in the composites was confirmed by XRD. The diffraction curves (CuK_α radiation) of all *Co–SiO₂* composites (Fig. 2) exhibit a set of reflections corresponding to Co_3O_4 (JCPDS 42–1467), no impurity phases were found. Particle sizes estimated on the base of coherent scattering area (CSA) correlate with pore sizes in composites. Thus, the average CSA size of Co_3O_4 calculated by the Rietveld refinement for *Co-SiO₂-mm* was found to be 4.7 ± 0.1 nm, for *Co-SiO₂-m* – 5.1 ± 0.1 nm, for *Co-SiO₂-lm* – 7.8 ± 0.1 nm, for opal – 25.1 ± 0.3 nm. From Table 1, it can be seen that the size of Co_3O_4 crystallites decreases with an increase in the specific surface area of the samples. Based on the XRD patterns of the samples, it can be concluded that the main crystalline phase in all composites is Co_3O_4. But the formation of amorphous oxides or cobalt silicates cannot be completely ruled out, especially in the micropores of silica. The silica surface in them is the most chemically active due to the greater curvature and, as a result, a large number of broken bonds in the silicon-oxygen framework.

Fig. 3 shows TEM images of the obtained *Co-SiO₂* composites. It is seen that the particles remain spherical after the introduction of cobalt. The dark spots observed on the surface of *Co-SiO₂-mm* particles probably contain an element with a large atomic number – Co (Fig. 3c). The TEM image of the particle region near one of these dark spots is shown in Fig. 4b. A crystalline material is observed on the silica surface, the crystallite size reaches 10 nm. The somewhat overestimated value of the CSA size of Co_3O_4 compared with the pore size in *SiO₂-mm* (Table 1) is possibly due to the presence of Co_3O_4 particles on the outer silica surface.. The crystallites observed in TEM images contribute to the calculated CSA size. At the same time, there are almost no Co_3O_4 crystallites on the surface of *SiO₂-m* and *SiO₂-lm* (Fig. 4b,c). In the enlarged image of the near-surface region of *Co-SiO₂-lm* (Fig. 4c,d), one can see crystallites

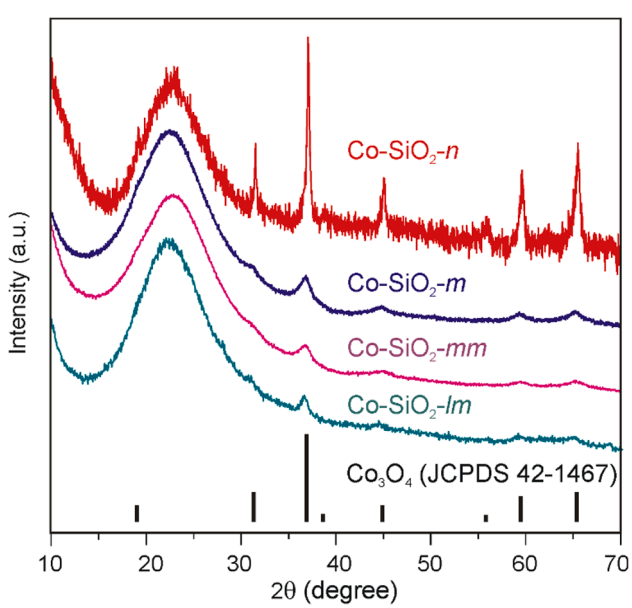

Fig. 2. XRD patterns of Co-SiO_2 composites.

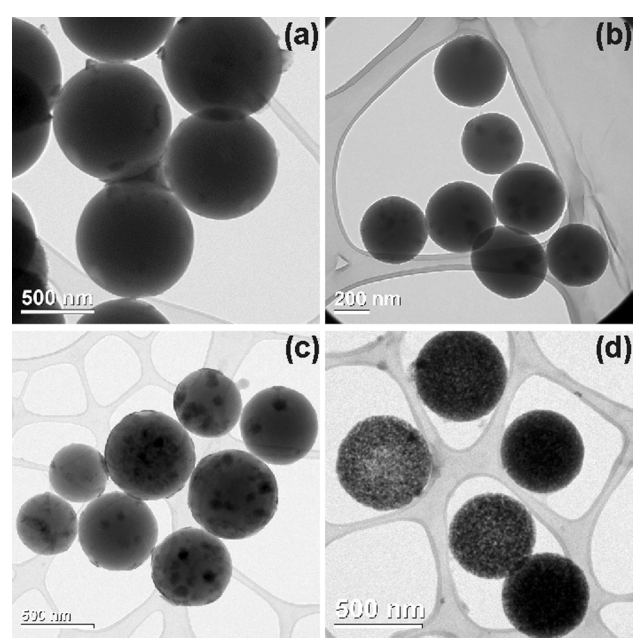

Fig. 3. TEM images: (a) Co-SiO_2-*n*, (b) Co-SiO_2-*m*, (c) Co-SiO_2-*mm*, (d) Co-SiO_2-*lm*.

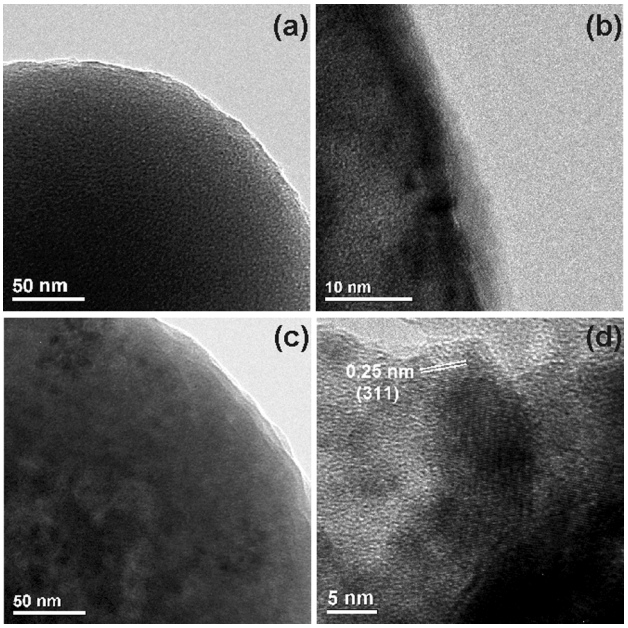

Fig. 4. Enlarged TEM images. (a) Co-SiO_2-*m*, (b) Co-SiO_2-*mm*, (c,d) Co-SiO_2-*lm*.

(dark areas) in the pores of a silica particle. The interplanar distance observed in the HRTEM image of one of the crystallites corresponds to d_{311} = 0.25 nm in Co_3O_4.

As one can see from Fig. 5a, cobalt oxide is located between *SiO_2-n* particles in the form of individual crystallites tens of nanometers in size and their groups, some of the interparticle pores in opal are completely filled (Fig. 5a). The microdiffraction pattern of the composite is shown in Fig. 5b. There is a set of reflections corresponding to polycrystalline Co_3O_4 (JCPDS 042–1467). Dark-field TEM (Fig. 5c) and HRTEM (Fig. 5d) images also demonstrate that the cobalt oxide in the opal interparticle pores is polycrystalline.

EDX analysis confirmed that all the composites consist of Si, O, Co. A typical EDX spectrum is shown in Fig. 6e. Fig. 6b-d shows the distribution maps for the main elements in the *Co-SiO_2-n* composite. There are objects tens of nanometers in size containing cobalt on the surface of *SiO_2-n* particles. An interparticle pore completely filled with cobalt oxide is also observed. Table 1 summarizes the results of structural studies of the obtained composites in comparison with initial silicas.

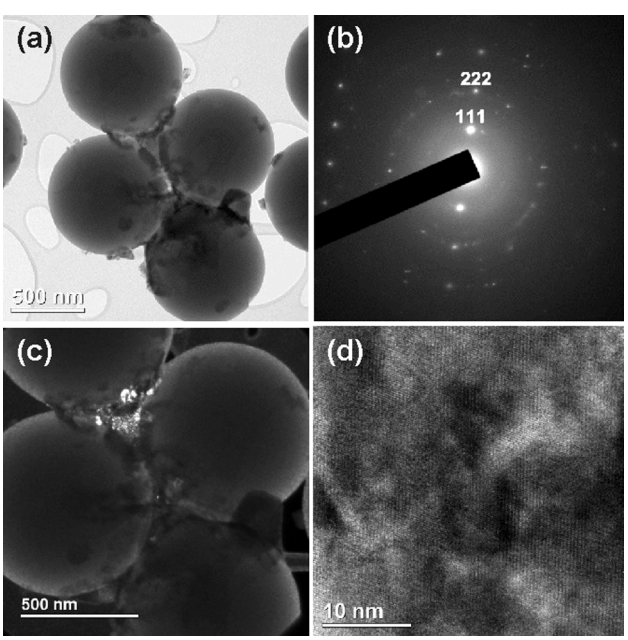

Fig. 5. TEM image of a fragment of *Co-SiO_2-n* composite (a), SA micro-diffraction pattern from an interparticle pore filled with cobalt oxide (b), dark-field image using (1 1 1) reflection of Co_3O_4 (c), HRTEM image of a filler (*d*). The Co_3O_4 reflections at panel (b) are indicated.

3.2. *XPS studies*

Only peaks attributed to oxygen, cobalt, silicon and carbon were observed in XP-spectra (Fig. S2) of *Co-SiO_2* composites. The concentrations of elements on the surface of the samples according to XPS data are listed in Table 2.

The O1s XP-spectra of all samples indicate the presence of two components with binding energies of 530.0–530.1 and 532.8–533.0 eV corresponding to oxygen in cobalt oxides (O—Co) and silica [35]. The O—Co fraction was 1–5% in all Co—SiO_2 as-prepared and spent samples (Table 3). A slightly higher content of oxygen bound to cobalt is typical for the samples with higher Co content (with respect to Si) on the surface of Co-*SiO_2-mm* and Co-*SiO_2-n* particles.

The Co2p XP-spectra are shown in Fig. 7. To analyze the fractions of Co^{2+} and Co^{3+} they were fitted with the CASAXPS software, the U2 Tougaard background in the binding energy range between about 775 and 812 eV was used (see Suppl. Section). For Co^{3+} component the constrains were built using the Co2p spectrum of $ScCo_{0.95}Fe_{0.05}O_3$ [36] that contained a major part of Co atoms in a Co^{3+} state. The Co^{2+} synthetic component was constructed based on the typical Co^{2+} spectrum with a high contribution of satellites, such as that of CoO or $Co(OH)_2$ [35]. The fractions of cobalt atoms in the oxidation states +2 (E_b = 781.1–781.7 eV) and +3 (E_b = 779.6–780.0 eV) derived from the decomposition of the spectra of the samples before and after catalysis are listed in Table 3, the accuracy of determining the fraction of cobalt atoms in various oxidation states was ± 5–10%.

The Co2p spectra of *Co-SiO_2-mm*, *Co-SiO_2-m*, and *Co-SiO_2-n* have a similar shape and show a significant contribution from both di- and trivalent cobalt. As can be seen from the Table 3 in all three cases Co^{3+} is predominant, however, the ratio of cobalt atoms in the two oxidation states is somewhat different. The highest value close to the ratio of these states in the Co_3O_4 structure was obtained for *Co-SiO_2-mm* and *Co-SiO_2-n* after catalysis. In contrast to the listed composites *Co-SiO_2-lm* contained mainly divalent cobalt, the fraction of Co^{3+} slightly increased after catalytic tests.

The difference in the electronic state of cobalt on the surface of *Co-SiO_2-lm* silica with the large mesopores from other samples may be due to the fact that some Si-O-Si bonds are broken under the action of H_2O_2 during synthesis forming coordination unsaturated silicon atoms. In this case the new Co-O-Si bonds can be more easily formed when a solution of cobalt nitrate (Co^{2+}) is introduced. The incorporation of Co^{2+} cations into SiO_2 should lead to the formation of compounds similar to that of cobalt phyllosilicates [37,38], which may be amorphous and, thus, are not detected by XRD. In this case, the oxidation of Co^{2+} cations to Co^{3+} during annealing will be difficult.

The additional information on the state and properties of cobalt oxides on the silica surface can be obtained using IR spectroscopy and TPR-H_2 studies of *Co-SiO_2*.

3.3. *FTIR spectroscopy studies*

Fig. 8 shows the FTIR spectra of different *Co-SiO_2* samples. The appearance of two distinctive bands at 560–566 cm^{-1} (ν_1) and 659–661 cm^{-1} (ν_2) caused by stretching vibrations of the metal – oxygen bond, confirms the formation of the Co_3O_4 spinel oxide [39–41]. The ν_1 band is associated with OB vibrations in the spinel lattice, where B indicates the Co^{3+} in an octahedral position, and the ν_2 band is attributed to the ABO_3 vibrations, where A stands for the Co^{2+} in a tetrahedral holes [39,40]. The highest frequency of stretching vibration band of octahedrally

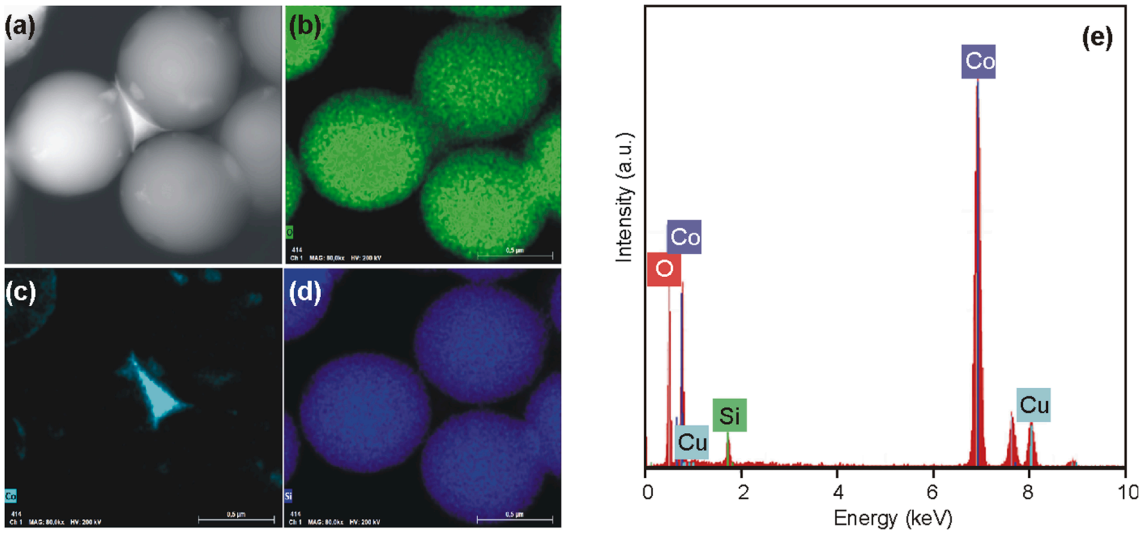

Fig. 6. HAADF STEM image (a), EDX maps of O (b), Co (c) and Si (d) in Co-SiO_2-*n* composite. EDX spectrum taken from an interparticle pore filled with cobalt oxide (e).

Table 2
Concentrations of elements on the surface of *Co-SiO₂* (at%) according to high-resolution XP-spectra.

Co-SiO₂		Co	O	C	Si
Co-SiO₂-lm	as-prepared	0.9	58.9	17.5	22.7
	spent	1.0	60.4	15.9	22.7
Co-SiO₂-mm	as-prepared	1.5	61.0	15.9	21.6
	spent	1.5	60.0	16.6	21.9
Co-SiO₂-m	as-prepared	0.3	60.8	17.1	21.8
	spent	0.3	61.1	16.9	21.7
Co-SiO₂-n	as-prepared	2.1	55.8	18.8	23.3
	spent	2.1	64.9	7.5	25.5

Table 3
Fractions of Co^{2+}, Co^{3+} (at%) and oxygen in cobalt oxides and silica on the surface of *Co-SiO₂* according to XPS data.

Co-SiO₂		Co^{2+}	Co^{3+}	Co^{3+}/Co^{2+}	Co/Si	O–Co/O–Si
Co-SiO₂-lm	as-prepared	92	8	0.1	0.040	0.01
	spent	84	16	0.2	0.044	0.01
Co-SiO₂-mm	as-prepared	39	61	1.6	0.069	0.03
	spent	39	61	1.6	0.068	0.03
Co-SiO₂-m	as-prepared	41	59	1.4	0.014	0.01
	spent	43	57	1.3	0.014	0.01
Co-SiO₂-n	as-prepared	45	55	1.2	0.090	0.05
	spent	37	63	1.7	0.083	0.04

coordinated Co^{3+} (ν_2), close to the frequency of pure Co_3O_4 [40], is observed in the *Co-SiO₂-n* containing the largest (25 nm) Co_3O_4 particles (Table 1). In other samples with an oxide particle size of 5–8 nm, the two bands slightly shift to a lower wave number due to a large number of defects at the surface of the smaller nanoparticles that weaken the Co – O bond strength [39]. The largest red shift of the Co-O vibration bands, as can be seen from Fig. 8, is observed for the *Co-SiO₂–m* and *Co-SiO₂–lm* samples, in which, according to XPS data and texture studies, the interaction of oxide particles with the silica surfaces is the strongest. As mentioned above, a significant decrease in the content of cobalt on the outer surface of *Co-SiO₂-m* (Table 2) indicates a greater dispersion of oxide particles and an increase in their interaction with the support up to the formation of cobalt-silicate structures. A decrease in the Co^{3+}/Co^{2+}

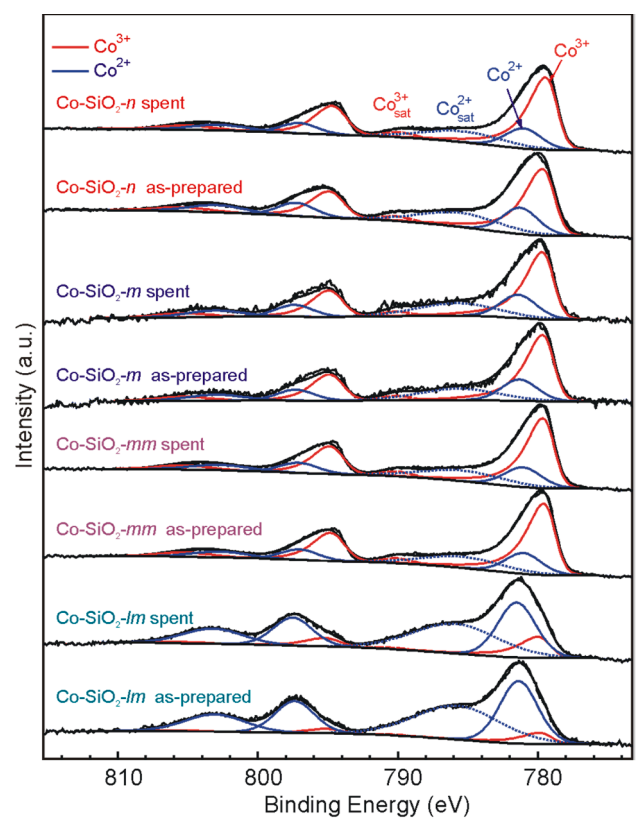

Fig. 7. Co2p XP-spectra of the *Co-SiO₂* samples before (as-prepared) and after catalysis (spent). Co^{2+}_{sat} and Co^{3+}_{sat} correspond to satellite substances.

ratio for the *Co-SiO₂-lm* as well as O–Co/O–Si ratios for *Co-SiO₂-lm* and *Co-SiO₂-m* (Table 3) confirms this assumption. The difference in the cobalt oxide particle size, their distribution and strength of interaction of cobalt atoms with silica surfaces in the mesoporous and large porous samples can be also revealed through their ability to be reduced.

3.4. TPR-H_2

Fig. 9 compares the measured TPR profiles of all *Co-SiO₂* samples. As

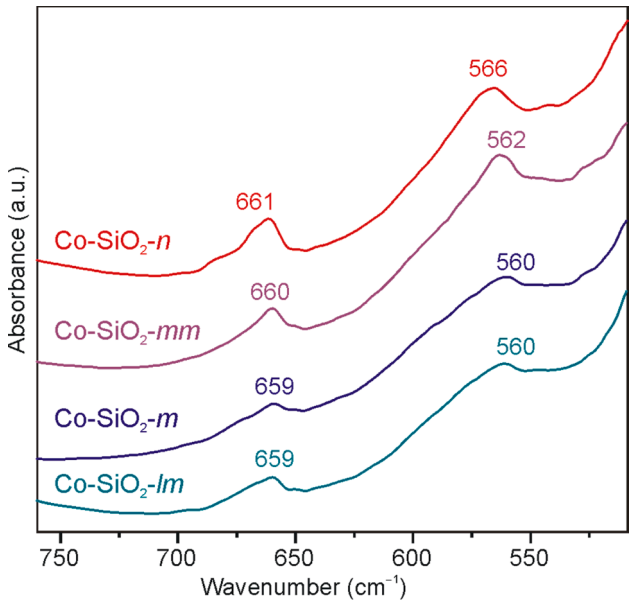

Fig. 8. FTIR spectra of *Co/SiO₂* samples in KBr.

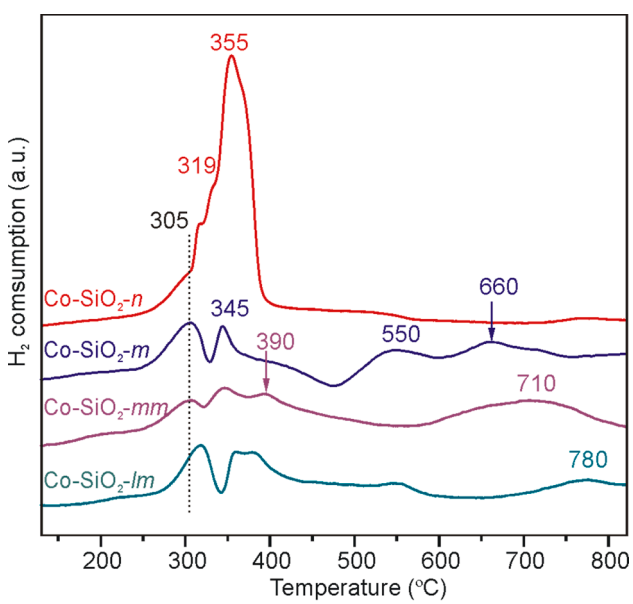

Fig. 9. TPR-profiles of Co-SiO_2 samples.

one can see, the profile for *Co-SiO₂-n* is very different from the profiles for other samples. It only contains two main H_2-consumptions in the temperature range 300–400 °C associated with the two-step reduction of Co_3O_4: Co_3O_4 to CoO (peak at temperatures 305–320 °C) and CoO to Co^0 (peak at temperatures 355–400 °C). This type of profile is characteristic for bulk cobalt oxide and large Co_3O_4 nanoparticles that weakly interact with the support [24,25,40,42,43]. In contrast to this, there are several peaks corresponding to hydrogen absorption in the range 350–600 °C in TPR profiles of three other samples of *Co-SiO₂ (m, mm, lm)*, the dispersion of oxide particles in which is much higher than that in *Co-SiO₂-n* (see Table 1). The manifestation of several peaks of the reduction of oxide particles in a wide temperature range is apparently associated with the presence of oxide particles of different sizes in the samples and also with their different distribution on the support surface (inside and outside the particles), which is reflected in their reducibility. An increase in the reduction temperature with a decrease in the particle size on the surface of silicate supports was observed, for example, in [42]. The high-temperature peaks above 550–780 °C are associated with Co species with stronger interaction with support [42,43]. A broad peak appeared in the TPR profiles of *Co-SiO₂-mm* and *Co-SiO₂-lm* at 710–780 °C can be assigned to the reduction of cobalt – phyllosilicates [37,42,43].

Summarizing the structural data, we can conclude that a fraction of cobalt oxide deposited on the outer surface of silica in comparison with that incorporated into pore space decreases in the series *Co-SiO₂-n* > *Co-SiO₂*-mm > *Co-SiO₂*-lm > *Co-SiO₂*-m. A size of Co_3O_4 crystallites on the surface of SiO_2 decreases from 25 to 5 nm in inverse proportion to the sillica surface area and correlates with pore size. Polycrystalline Co_3O_4 aggregates in *Co-SiO₂-n* are mostly located in the interparticle space of the opal structure. Thus, the morphological characteristics of silica determine the cobalt oxide particle size, their distribution in the support structure, and, correspondingly, the degree of cobalt species – silica interaction. This is reflected in the electronic state of cobalt, reducibility of *Co-SiO₂* samples and their behavior in catalysis.

3.5. Catalytic activity in oxidation of CO

The temperature dependences of CO conversion in an inert atmosphere for *Co-SiO₂* composites are shown in Fig. 10a. It can be seen that the oxidation of CO is quantitatively carried out in the temperature range 150–210 °C. Multiple tests in heating–cooling modes have shown that all samples are stable. Deviations in temperatures for 10 and 50% conversion of CO (T_{10} and T_{50}) do not exceed ± 3 degrees in 4 successive cycles. To characterize the catalysts, we used T_{10} and T_{50} temperatures reached during the second test cycle. The values of T_{10} and T_{50} for all studied *Co-SiO₂* composites are listed in Table 4. As can be seen from these data *Co-SiO₂-n* exhibited the highest activity in CO oxidation. The high activity of this sample obtained on silica (synthetic opal) with the lowest specific surface area was unexpected.

Fig. 10b shows temperature dependences of the CO conversion in CO-PROX reaction. Characteristic temperatures T_{10} and T_{50} of CO oxidation in a H_2-rich gas mixture are given in Table 4. As one can see from a comparison of data in Fig. 10 (a and b) and Table 4 the temperature dependences of CO conversion in the presence of hydrogen are shifted to higher temperatures. This is due to the competitive adsorption of CO and H_2 molecules on active sites on the surface of cobalt oxide and their simultaneous oxidation with the formation of CO_2 and H_2O. The mechanism of selective CO oxidation and the nature of active sites on the surface of Co_3O_4 are discussed in detail in [8–10]. It is known that the activation energy of CO oxidation is lower than that of hydrogen [17]. Therefore, the predominant process at relatively low temperatures is the oxidation of CO. With an increase in temperature, the contribution of the competitive H_2 oxidation becomes significant, and the CO conversion decreases. As seen from Fig. 10b the temperatures of the maximum CO conversion for the studied samples are very different, the corresponding T_{max} values are listed in Table 4.

The *Co-SiO₂-n* sample also turned out to be the most active in CO-PROX. The CO conversion reaches its maximum value of 90% already at 170 °C. At the same time, the most large-porous *Co-SiO₂-lm* is the least active in CO-PROX as well as in the case of the total oxidation. The maximum CO conversion in PROX for this sample is only 73% at temperature above 230 °C.

According to these data the synthesized composites are arranged in a row *Co-SiO₂-n* > *Co-SiO₂-mm* > *Co-SiO₂-m* > *Co-SiO₂-lm* both in the absence and in the presence of hydrogen. Recently, a similar effect of the support structure on the efficiency of catalysts in the CO-PROX was observed in [44]. Using CuO-CeO_2/SiO_2 the authors showed that catalysts with a specific surface area $S = 20\ m^2/g$ possessed higher activity compared to the same samples with S up to 650 m^2/g. A high (>90%) CO conversion was observed in the same temperature range 140–210 °C.

Based on structural data, TPR-H_2 and spectral (XP and FTIR) studies of *Co-SiO₂* we can conclude that a reason for such different catalytic properties of *Co-SiO₂* with different morphologies may be associated with the size of cobalt oxide particles, their distribution and Co

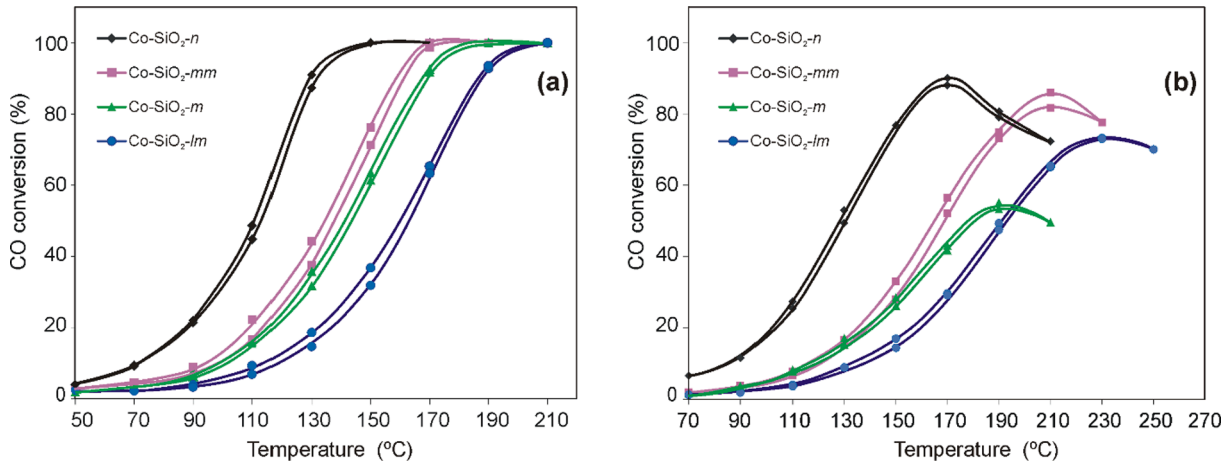

Fig. 10. The temperature dependences of CO conversion for the *Co-SiO$_2$* samples in the reaction of CO oxidation in the mixture (a) 1% CO, 1% O_2, 98% He and (b) 1% CO, 1% O_2, 49% H_2, 49% He (the heating and cooling cycles are displayed).

Table 4
T_{10} and T_{50} (°C) in the CO oxidation and PROX on *Co-SiO$_2$* catalysts, and T_{max} temperatures at which maximum CO conversion (CO_{max}, %) is reached in the presence of H_2.

Catalyst		Co-SiO$_2$-*n*	Co-SiO$_2$-*mm*	Co-SiO$_2$-*m*	Co-SiO$_2$-*lm*
CO-OX[a)]	T_{10}	72	98	100	120
	T_{50}	112	140	145	162
CO-PROX[b)]	T_{10}	88	118	120	138
	T_{50}	128	165	180	195
	T_{max}	170	210	190	230
	CO_{max}, %	90	86	55	73

[a)] In 1 vol% CO, 1 vol% O_2, 98 vol% He at a total flow of 10 mL/min
[b)] In 1 vol% CO, 1 vol% O_2, 49 vol% H_2, 49 vol% He at a total flow of 10 mL/min

electronic state on the surface of silica. The most active *Co-SiO$_2$-n* contains the largest Co_3O_4 particles in the interparticle space of opal, in this case the Co/Si ratio reaches the largest value (0.09, Table 3). These particles interact less with the silica support and can be easier reduced. The maximum Co^{3+}/Co^{2+} ratio during the tests is also achieved on this most active *Co-SiO$_2$-n*. A correlation between catalytic activity and reducibility in the CO oxidation was found for a number of catalysts based on cobalt oxides [16,39,45,46].

At the same time a possibility of the participation of CoO or Co^{2+} cations within oxo complexes as active centers of adsorption and catalysis is also discussed [19–21]. However, the *Co-SiO$_2$-lm* strongly different in composition from the others, and containing mostly Co^{2+}, turned out to be less active in CO oxidation.

Comparison of XPS data for catalysts before and after reaction (Fig. 7 and Table 3) shows that the Co^{3+} fraction slightly increases for *Co-SiO$_2$-n* and *Co-SiO$_2$-lm* and doesn't change for the *Co-SiO$_2$-m* and *Co-SiO$_2$-mm*. The Co/Si and O-Co/O-Si ratios change very slightly, which indicates high stability of *Co-SiO$_2$* composites during catalysis.

The greatest changes in the activity upon the introduction of hydrogen into the reaction mixture are observed for the *Co-SiO$_2$-m* composite. Fig. 10b and Table 4 show that the maximum CO conversion on this catalyst in CO-PROX reaction reaches only 55%, and then begins to decrease. At the same time, the maximum CO conversion is 86% at 210 °C for the *Co-SiO$_2$-mm* composite having a similar activity in the absence of hydrogen (see Fig. 10a). It should be noted that the electronic state of cobalt in both composites corresponds to Co_3O_4 oxide (see Table 3). The observed significant difference in the activity of *Co-SiO$_2$-m* and *Co-SiO$_2$-mm* in CO-PROX is presumably associated with the different distribution of cobalt oxide nanoparticles on the catalyst surface. Indeed, from the Table 2 it is seen that the surface Co content for the *Co-SiO$_2$-m* composite is only 0.3 at%, while for the *Co-SiO$_2$-mm* this value is 5 times higher (1.5 at%). Apparently, the pore size of the first sample, which is almost twice larger, promotes the formation of Co_3O_4 nanoparticles not only on the outer surface, but also inside the pores of the *Co-SiO$_2$-m* catalyst, which is confirmed by TEM (Figs. 3 and 4). Probably, the higher dispersion of Co_3O_4 nanoparticles facilitates more efficient adsorption and activation of hydrogen on their surface and, as a result, a decrease in the selectivity of CO_2 formation.

On the contrary, larger Co_3O_4 nanoparticles in the interparticle pores of opal on the surface of *Co-SiO$_2$-n* (Fig. 5) turned out to be surprisingly more active not only in the CO oxidation but also in CO-PROX reaction. Possibly, the formation of agglomerates of relatively large (~25 nm) cobalt oxide nanoparticles separated by silica particles provides favorable conditions for electron transfer processes associated with the reversible transition in the Co^{3+}/Co^{2+} redox couple when interacting with CO and oxygen molecules, respectively. According to XPS a slight increase in the fraction of Co^{3+} compared to Co^{2+} is observed for the *Co-SiO$_2$-n* catalyst after the reaction. It also attests to the fact that the formation of Co_3O_4 agglomerates inside the macropores between SiO_2 particles of opal may stabilize the oxidized state Co^{3+} in such composites. A possible interaction of smaller Co_3O_4 nanoparticles with silica support will not facilitate such stabilization. A similar conclusion about the importance of Co_3O_4 nanoparticles - support interactions was made on the example of Al_2O_3 in [45]. A catalyst with the weak particle - support interaction provided both a higher yield of CO_2 and selectivity in CO-PROX reaction compared to the sample where this interaction was stronger.

Note that a slight increase in the fraction of Co^{3+} after the reaction occurs not only in the most active *Co-SiO$_2$-n* catalyst, but also in the least active – *Co-SiO$_2$-lm*. In accordance with XPS and XRD data the number of Co_3O_4 nanoparticles in the *Co-SiO$_2$-lm* composite is significantly less than in the other *Co-SiO$_2$* composites, and their size is close to 8 nm which is higher than that in the *Co-SiO$_2$-m* and *Co-SiO$_2$-mm*. As a result of the larger size of oxide nanoparticles and correspondingly smaller effect of the interaction with support, redox processes in the Co^{2+}/Co^{3+} couple under the action of O_2, CO, and H_2 seem to proceed a little easier. However, *Co-SiO$_2$-lm* composite is less active because initially most of the cobalt on this support is present in the oxidation state of + 2 (Table 3) which is unfavorable for oxidation reactions.

The characteristics of the *Co-SiO$_2$* composites (Table 4) correspond to or exceed those for catalysts based on supported cobalt oxides. For example, the use of high-loaded 10% Co_3O_4/Al_2O_3 under similar conditions makes it possible to achieve the maximum CO conversion in CO-PROX reaction of 98% at 170 °C [45]. On catalysts with lower cobalt content (1–7 wt% of CoO) with the use of catalytically active CeO_2 as a

support the CO conversion reached only 67–84% at 230–240 °C [46]. For Co_3O_4 nanoparticles [8] the temperatures for 10% CO conversion in the absence of H_2 were 100 and 150 °C depending on the particle morphology. The maximum CO conversion in PROX for more active Co_3O_4 nanoplates was only 75% at 170 °C. For comparison, the best *Co-SiO₂-n* catalyst (2.9% Co) based on synthetic opal first prepared in this work provides the 90% conversion of CO at 170 °C. Another important advantage of silicas decorated with cobalt oxides is maintenance of their structural and catalytic properties in repeated cyclic tests both in the absence and in the presence of hydrogen. The stabilization of the most active electronic and coordination state of cobalt under conditions of selective CO oxidation is an important task on the way of creating effective catalysts based on cobalt oxides.

4. Conclusion

To study the impact of silica morphology on the Co/SiO_2 structure and catalytic activity in the CO oxidation and CO-PROX in a H_2-rich gas mixture non-porous and porous spherical silica particles with pores 0.6–30 nm in size were synthesized. They were decorated with cobalt oxides using the capillary impregnation method. The Co content in all *Co-SiO₂* composites was about 3 wt%. The composition and structure of the obtained materials were studied using nitrogen adsorption porosimetry, TEM, EDX, XRD, XPS, FTIR spectroscopy and TPR methods. It is shown that the obtained *Co-SiO₂* composites are microporous (*Co-SiO₂-mm*, S = 1200 m^2/g), mesoporous with pores of a few nanometers (*Co-SiO₂-m*, S = 700 m^2/g) and tens of nanometers (*Co-SiO₂-lm*, S = 400 m^2/g) and macroporous (opal grown from non-porous *Co-SiO₂-n*, S = 10 m^2/g, interparticle pores up to 300 nm) materials. According to XRD data, the main crystalline phase in all composites was identified as Co_3O_4, the particle size is inversely proportional to the sillica surface area and correlates with pore size. A fraction of cobalt oxide deposited on the outer silica surface in comparison with that incorporated into pore space decreases in the series *Co-SiO₂-n* > *Co-SiO₂*-mm > *Co-SiO₂*-lm > *Co-SiO₂*-m. Co-decorated silicas were active in the CO oxidation and CO-PROX reaction. The oxidation of CO proceeds quantitatively in the temperature range 150–210 °C. Both in the absence and in the presence of H_2 the activity of $Co\text{-}SiO_2$ composites improves with increasing atomic ratios of Co/Si and Co^{3+}/ Co^{2+} on the silica surface. According to catalytic activity, the synthesized composites can be arranged in the order *Co-SiO₂-n* > *Co-SiO₂-mm* > *Co-SiO₂-m* > *Co-SiO₂-lm*. Using the synthetic opal grown by sedimentation of non-porous silica *SiO₂-n* particles with the lowest specific surface area as a support for cobalt oxides resulted in the most active catalyst. CO conversion reaches 100% at 150 °C in the absence of hydrogen and 90% at 170 °C in the PROX reaction. The highest activity of Co_3O_4 aggregates between spherical silica particles in *Co-SiO₂-n* correlates with their reducibility. Large Co_3O_4 nanoparticles weakly interacting with non-porous silica and containing the largest Co^{3+} fraction provide a higher yield of CO_2 in CO-PROX reaction. In contrast to this *Co-SiO₂-lm* containing mainly Co^{2+} species was the least active.

All $Co\text{-}SiO_2$ composites were stable in the reducing conditions during CO-PROX reaction, the CO conversion did not decrease after multiple repeated catalytic cycles. This study shows a new economically promising way to synthesize active and stable catalysts based on cobalt oxides. The fact of unusually high activity of the new material - synthetic opal decorated with cobalt oxides deserves great attention from the point of view of understanding the mechanism of action of cobalt oxides in catalysis and their applications in the wide range of redox reactions.

CRediT authorship contribution statement

Daniil A. Eurov: Resources, Investigation, Writing – original draft, Writing – review & editing. **Tatiana N. Rostovshchikova:** Conceptualization, Funding acquisition, Supervision, Writing – review & editing. **Marina I. Shilina:** Investigation, Data curation, Writing – review & editing. **Demid A. Kirilenko:** Investigation, Validation, Writing – review & editing. **Maria V. Tomkovich:** Investigation, Formal analysis. **Maria A. Yagovkina:** Visualization, Investigation. **Olga V. Udalova:** Investigation, Validation, Writing – review & editing. **Igor Yu. Kaplin:** Investigation, Formal analysis. **Igor A. Ivanin:** Investigation, Validation. **Dmitry A. Kurdyukov:** Conceptualization, Supervision, Project administration, Writing – review & editing.

Declaration of Competing Interest

The authors declare that they have no known competing financial interests or personal relationships that could have appeared to influence the work reported in this paper.

Acknowledgements

Synthesis and analysis of physical and chemical characteristics of materials were financed within the framework of the state budget agreement (Grant No.0040-2019-0012). Catalytic tests were carried out in accordance with State assignments on topics No. AAAA-A21-121011590090-7 and 0082-2019-0011 “Fundamental laws of heterogeneous and homogeneous catalysis”. Transmission electron microscopy studies were performed using the equipment of the Federal Center for Collective Use “Materials Science and Diagnostics in Advanced Technologies”. TXRF and XPS studies were carried out using equipment of Lomonosov Moscow State University (Program of MSU Development).

Appendix A. Supplementary material

Supplementary data to this article can be found online at https://doi.org/10.1016/j.apsusc.2021.152121.

References

[1] H.-J. Freund, G. Meijer, M. Scheffler, R. Schlögl, M. Wolf, CO Oxidation as a prototypical reaction for heterogeneous processes, Angew. Chem. Int. Ed. 50 (43) (2011) 10064–10094.
[2] S. Royer, D. Duprez, Catalytic oxidation of carbon monoxide over transition metal oxides, ChemCatChem 3 (1) (2011) 24–65.
[3] P. Jing, X. Gong, B. Liu, J. Zhang, Recent advances in synergistic effect promoted catalysts for preferential oxidation of carbon monoxide, Catal, Sci. Technol. 10 (4) (2020) 919–934.
[4] E.D. Park, D. Lee, H.C. Lee, Recent progress in selective CO removal in a H_2-rich stream, Catal. Today 139 (4) (2009) 280–290.
[5] F. Marin, C. Descormea, D. Duprez, Supported base metal catalysts for the preferential oxidation of carbon monoxide in the presence of excess hydrogen (PROX), Appl. Catal. B 58 (2005) 175–183.
[6] Z. Zhao, R. Jin, T. Bao, X. Lin, G. Wang, Mesoporous ceria-zirconia supported cobalt oxide catalysts for CO preferential oxidation reaction in excess H_2, Appl. Catal. B 110 (2011) 154–163.
[7] S. Dey, G.C. Dhal, The catalytic activity of cobalt nanoparticles for low-temperature oxidation of carbon monoxide, Mater. Today Chem. 14 (2019), 100198.
[8] Y.I. Choi, H.J. Yoon, S.K. Kim, Y. Sohn, Crystal-facet dependent CO oxidation, preferential oxidation of CO in H_2-rich, water-gas shift reactions, and supercapacitor application over Co_3O_4 nanostructures, Appl. Catal. A 519 (2016) 56–67.
[9] W. Huan, J. Li, J. Ji, M. Xing, In situ studies on ceria promoted cobalt oxide for CO oxidation, Chin. J. Catal. 40 (2019) 656–663.
[10] L. Lukashuk, K. Föttinger, E. Kolar, C. Rameshan, D. Teschner, M. Hävecker, A. Knop-Gericke, N. Yigit, H. Li, E. McDermott, M. Stöger-Pollach, G. Rupprechter, Operando XAS and NAP-XPS studies of preferential CO oxidation on Co_3O_4 and CeO_2-Co_3O_4 catalysts, J. Catal. 344 (2016) 1–15.
[11] S. Varghese, M.G. Cutrufello, E. Rombi, C. Cannas, R. Monaci, I. Ferino, CO oxidation and preferential oxidation of CO in the presence of hydrogen over SBA-15-templated CuO-Co_3O_4 catalysts, Appl. Catal. A 443–444 (2012) 161–170.
[12] A.A. Firsova, T.I. Khomchenko, O.N. Sil'chenkova, V.N. Korchak, Oxidation of carbon monoxide in the presence of hydrogen on the CuO, CoO, and Fe_2O_3 oxides supported on ZrO_2, Kinet. Catal. 51 (2010) 317–329.
[13] Z. Zhao, X. Lin, R. Jin, Y. Dai, G. Wang, High catalytic activity in CO PROX reaction of low cobalt-oxide loading catalysts supported on nano-particulate CeO_2-ZrO_2 oxides, Catal. Commun. 12 (15) (2011) 1448–1451.
[14] M. Hattori, S. Nakakura, H. Katsui, T. Goto, M. Ozawa, High CO reactivity of cobalt oxide catalyst deposited on alumina powders by rotary chemical vapor deposition, Mater. Lett. 284 (2021), 128922.

[15] H.M.A. Hassan, M.A. Betiha, R.F.M. Elshaarawy, M. Samy El-Shall, Promotion effect of palladium on Co_3O_4 incorporated within mesoporous MCM-41 silica for CO oxidation, Appl. Surf. Sci. 402 (2017) 99–107.

[16] M.I. Shilina, T.N. Rostovshchikova, S.A. Nikolaev, O.V. Udalova, Polynuclear Co-oxo cations in the catalytic oxidation of CO on Co-modified ZSM-5 zeolites, Mater. Chem. Phys. 223 (2019) 287–298.

[17] P. Gawade, B. Bayram, A.-M.C. Alexander, U.S. Ozkan, Preferential oxidation of CO (PROX) over CoO_x/CeO_2 in hydrogen-rich streams: Effect of cobalt loading, Appl. Catal. B 128 (2012) 21–30.

[18] S. Dey, G.C. Dhal, D. Mohan, R. Prasad, Synthesis of highly active cobalt catalysts for low temperature CO oxidation, Chem. Data Collect. 24 (2019), 100283.

[19] L. Zhang, L. Dong, W. Yu, L. Liu, Y. Deng, B. Liu, H. Wan, F. Gao, K. Sun, L. Dong, Effect of cobalt precursors on the dispersion, reduction, and CO oxidation od CoO_x/γ-Al_2O_3 catalysts calcined in N_2, J. Colloid Interface Sci. 355 (2011) 464–471.

[20] S.A. Singh, G. Madras, Detailed mechanism and kinetic study of CO oxidation on cobalt oxide surfaces, Appl. Catal. A 504 (2015) 463–475.

[21] R. Molavi, R. Safaiee, M.H. Sheikhi, N. Hassani, Theoretical perspective on CO oxidation over small cobalt oxide clusters, Chem. Phys. Lett. 767 (2021), 138361.

[22] S. Angelos, E. Johansson, J. F. Stoddart, J. I. Zink, Mesostructured silica supports for functional materials and molecular machines, Adv. Funct. Mater. 17 (14) (2007) 2261–2271.

[23] D. Zhao, Y. Wan, W. Zhou, Ordered Mesoporous Materials, Wiley (2013) 523.

[24] C.-B. Wang, C.-W. Tang, H.-C. Tsai, S.-H. Chien, Characterization and Catalytic Oxidation of Carbon Monoxide Over Supported Cobalt Catalysts, Catal. Lett. 107 (3-4) (2006) 223–230.

[25] T.M. Nyathi, M.I. Fadlalla, N. Fischer, A.P.E. York, E.J. Olivier, E.K. Gibson, P. P. Wells, M. Claeys, Support and gas environment effects on the preferential oxidation of carbon monoxide over Co_3O_4 catalysts studied in situ, Appl. Catal. B: Environmental. 297 (2021), 120450.

[26] I. Lopes, A. Davidson, C. Thomas, Calibrated Co_3O_4 nanoparticles patterned in SBA-15 silicas: Accessibility and activity for CO oxidation, Catal. Commun. 8 (2007) 2105–2109.

[27] L. Kuboňová, P. Peikertová, K. Mamulová Kutláková, K. Jirátová, G. Słowik, L. Obalová, P. Cool, Catalytic activity of cobalt grafted on ordered mesoporous silica materials in N_2O decomposition and CO oxidation, Molecul. Catal. 437 (2017) 57–72.

[28] P.A. Robles-Dutenhefner, K.A. da Silva Rocha, E.M.B. Sousa, E.V. Gusevskay, Cobalt-catalyzed oxidation of terpenes: Co-MCM-41 as an efficient shape-selective heterogeneous catalyst for aerobic oxidation of isolongifolene under solvent-free conditions, J. Catal. 265 (2009) 72–79.

[29] E.Y. Trofimova, A.E. Aleksenskii, S.A. Grudinkin, I.V. Korkin, D.A. Kurdyukov, V. G. Golubev, Effect of tetraethoxysilane pretreatment on synthesis of colloidal particles of amorphous silicon dioxide, Colloid J. 73 (4) (2011) 546–550.

[30] E.Y. Trofimova, D.A. Kurdyukov, S.A. Yakovlev, D.A. Kirilenko, Y.A. Kukushkina, A.V. Nashchekin, A.A. Sitnikova, M.A. Yagovkina, V.G. Golubev, Monodisperse spherical mesoporous silica particles: fast synthesis procedure and fabrication of photonic-crystal films, Nanotechnology 24 (2013), 155601.

[31] D.A. Kurdyukov, D.A. Eurov, D.A. Kirilenko, J.A. Kukushkina, V.V. Sokolov, M. A. Yagovkina, V.G. Golubev, High-surface area spherical micro-mesoporous silica particles, Micropor. Mesopor. Mat. 223 (2016) 225–229.

[32] D.A. Eurov, D.A. Kirilenko, M.V. Tomkovich, T.N. Rostovshchikova, M.I. Shilina, O.V. Udalova, D.A. Kurdyukov, Porous silica particles modified in NH_3+H_2O+H_2O mixture: structure, filling with cobalt oxide and activity in CO conversion, Inorg. Mater. 57 (2021) 906–912.

[33] S.J. Gregg, K.S.W. Sing, Adsorption, Surface Area and Porosity, 2nd Ed., Academic Press, 1982, p. 303 p..

[34] V.N. Bogomolov, T.M. Pavlova, Three-dimensional cluster lattices, Semiconductors 29 (1995) 428–439.

[35] M.C. Biesinger, B.P. Payne, A.P. Grosvenor, L.W.M. Lau, A.R. Gerson, R.S.C. Smart, Resolving surface chemical states in XPS analysis of first row transition metals, oxides and hydroxides: Cr, Mn, Fe, Co and Ni, Appl. Surf. Sci. 257 (2011) 2717–2730.

[36] Y.A. Teterin, A.V. Sobolev, A.A. Belik, Y.S. Glazkova, K.I. Maslakov, V. G. Yarzhemskii, A.Y. Teterin, K.E. Ivanov, I.A. Presnyakov Electronic structure of cobaltites $ScCo_{1-x}Fe_xO_3$ (x=0,0.05) and $BiCoO_3$: X-ray photoelectron spectroscopy, J. Exp. Theor. Phys. 128 (2019) 899–908.

[37] I. Puskas, T.H. Fleisch, J.B. Hall, B.L. Meyers, R.T. Roginski, Metal-support interactions in precipitated, magnesium-promoted cobalt-silica catalysts, J. Catal. 134 (2) (1992) 615–628.

[38] A. Barbier, A. Hanif, J.A. Dalmon, G.A. Martin, Preparation and characterization of well-dispersed and stable Co/SiO_2 catalysts using the ammonia method, Appl. Catal. A 168 (1998) 333–343.

[39] Y.-Z. Wang, Y.-X. Zhao, C.-G. Gao, D.-S. Liu, Preparation and catalytic performance of Co_3O_4 catalysts for low-temperature CO oxidation, Catal. Lett. 116 (3-4) (2007) 136–142.

[40] C.-W. Tang, C.-B. Wang, S.-H. Chien, Characterization of cobalt oxides studied by FT-IR, Raman, TPR and TG-MS, Termochimica Acta 473 (1-2) (2008) 68–73.

[41] Ž. Chromčáková, L. Obalová, F. Kovanda, D. Legut, A. Titov, M. Ritz, D. Fridrichová, S. Michalik, P. Kuśtrowski, K. Jirátová, Effect of precursor synthesis on catalytic activity of Co_3O_4 in N_2O decomposition, Catalysis Today 257 (2015) 18–25.

[42] G. Prieto, A. Martinez, P. Concepcion, R. Moreno-Tost, Cobalt particle size effects in Fischer-Tropsch synthesis: structural and in situ spectroscopic characterisation on reverse micelle-synthesised Co/ITQ-2 model catalysts, J. Catal. 266 (2009) 129–144.

[43] K. Klaigaew, C. Samart, C. Chaiya, Y. Yoneyama, N. Tsubaki, P. Reubroycharoen, Effect of preparation methods on activation of cobalt catalyst supported on silica fiber for Fischer-Tropsch synthesis, Chem. Engineering J. 278 (2015) 166–173.

[44] I.S. Tiscornia, A.M. Lacoste, L.E. Gomez, A.V. Boix, CuO-CeO_2/SiO_2 coating on ceramic monolith: Effect of the nature of the catalyst support on CO preferential oxidation in a H_2-rich stream, Int. J. Hydrogen Energy 45 (2020) 6636–6650.

[45] T.M. Nyathi, N. Fischer, A.P.E. York, D.J. Morgan, G.J. Hutchings, E.K. Gibson, P. P. Wells, C.R.A. Catlow, M. Claeys, Impact of nanoparticle-support interactions in Co_3O_4/Al_2O_3 catalysts for the preferential oxidation of carbon monoxide, ACS Catal. 9 (2019) 7166–7178.

[46] A.A. Firsova, T.I. Khomenko, A.N. Il'ichev, V.N. Korchak, Co oxidation with oxygen in the presence of hydrogen on CoO/CeO_2 and $CuO/CoO/CeO_2$ catalysts, Kinet. Catal. 49 (2008) 682–691.